

Weierstraß–Institut für Angewandte Analysis und Stochastik

im Forschungsverbund Berlin e.V.

Preprint

ISSN 0946 – 8633

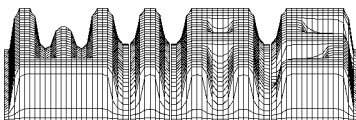
Instabilities of lasers with moderately delayed optical feedback

Matthias Wolfrum, Dmitry Turaev

submitted: 8 Feb 2002

Weierstrass Institute
for Applied Analysis
and Stochastics
Mohrenstr. 39
D - 10117 Berlin
Germany
wolfrum@wias-berlin.de
turaev@wias-berlin.de

Preprint No. 714
Berlin 2002



Key words and phrases. delay differential equations, bifurcation analysis.

Edited by
Weierstraß-Institut für Angewandte Analysis und Stochastik (WIAS)
Mohrenstraße 39
D — 10117 Berlin
Germany

Fax: + 49 30 2044975
E-Mail (X.400): c=de;a=d400-gw;p=WIAS-BERLIN;s=preprint
E-Mail (Internet): preprint@wias-berlin.de
World Wide Web: <http://www.wias-berlin.de/>

Abstract

We Perform a bifurcation analysis of the Lang-Kobayashi system for a laser with delayed optical feedback in the situation of moderate delay times. Using scaling methods, we are able to calculate the primary bifurcations, leading to instability of the stationary lasing state. We classify different types of pulsations and identify a codimension two bifurcation of fold-Hopf interaction type as the organizing centre for the appearance of more complicated dynamics.

1 Introduction

Delayed optical feedback is one of the fundamental mechanisms, leading to instability and complicated dynamics in semiconductor lasers [12]. Especially the situation of large delay times has been studied extensively, both numerically and in experiments. In this case a complicated behaviour with high dimensional chaos is observed (so called low-frequency fluctuations [2]). In contrast to that, the situation of smaller feedback time, as it arises for example in integrated multi-section devices, has received much less attention.

In this paper, we will perform a bifurcation analysis for the Lang-Kobayashi system, restricted to the case of small and moderate feedback times. This will lead to a refined investigation of how the stationary state of the laser without feedback changes, loses its stability, and with growing feedback gives rise to more complicated behaviour. Our approach will provide a unifying and more detailed view to earlier results of Tromborg e.a. [13, 7], Petermann and Tager [11], and Erneux e.a. [8, 9, 3] for the Lang-Kobayashi system, as well as to results for multi-section lasers [1, 14]. Using scaling techniques, we will calculate the primary bifurcations from stationary lasing, distinguish different types of pulsations, and discuss a codimension two bifurcation as an organizing centre for the appearance of more complicated dynamics. Especially, we discuss the role of the resonator properties of the compound cavity for the dynamical behaviour of the system.

The behaviour of a single moded laser under the influence of delayed optical feedback can be described by the Lang-Kobayashi rate equations

$$\frac{dE}{dT} = \frac{1}{2}(\mathcal{G}(N, |E(T)|^2) - \frac{1}{\tau_p}) \cdot E(T) + \kappa e^{-i\omega_0\tau_f} \cdot E(T - \tau_f) \quad (1)$$

$$\frac{dN}{dT} = I - \frac{N}{\tau_c} - \text{Re}[\mathcal{G}(N, |E(T)|^2)] \cdot |E(T)|^2 \quad (2)$$

for the field amplitude E and the carrier density N [6]. The lasing frequency ω_0 of the laser without feedback is used as the reference frequency, i.e. the actual field amplitude is given by $\frac{1}{2}(E(T)e^{i\omega_0 T} + \text{c.c.})$. With I we denote the pumping current, and $\mathcal{G}(N, |E(T)|^2)$ is the complex gain function; τ_p, τ_c, τ_f are photon lifetime, carrier lifetime, and feedback time. The feedback rate κ has to be computed from the reflectivities, external losses, and the internal round trip time (see [11]). Equations of this type have been shown to be able to describe a variety of different dynamical phenomena in good coincidence with experimental data. Moreover they can serve as a prototype model to obtain an understanding of the basic mechanisms leading to complicated dynamics in the presence of delayed optical feedback.

To adopt the general system (1), (2) to our more specific situation, we will now introduce some simplifications and rescalings. We want here to restrict our attention to situations, where the external round-trip time is not more than one order of magnitude bigger than the internal round-trip time. Consequently, we may rescale the time as

$$t := \frac{T}{\tau_f}.$$

Since we are not interested in high intensity effects, we neglect nonlinear gain saturation and linearize the complex gain function around the stationary lasing state ω_0, N_0 of the laser without feedback

$$\mathcal{G}(N, |E(T)|^2) - \frac{1}{\tau_p} := G_N(1 + i\alpha)(N - N_0)$$

With the rescaling

$$N_{res} := \frac{1}{2}\tau_f G_N(N - N_0)$$

we have simplified the optical equation to

$$\frac{dE(t)}{dt} = (1 + i\alpha)N_{res} \cdot E(t) + \eta e^{-i\phi} \cdot E(t - 1), \quad (3)$$

with the effective feedback strength $\eta := \kappa\tau_f$. The phase factor $\phi := \omega_0\tau_f$ we want to treat as an additional free parameter. This seems naturally to us in the sense of a separation of scales: already slight changes of τ_f change the phase condition completely, while all other parameters are not changed significantly.

We introduce now the above rescalings into the carrier equation, and additionally set

$$E_{res} := \sqrt{\tau_c G_N} E.$$

Of course, this rescaling of E does not affect the linear equation (3). From this we obtain

$$\frac{dN_{res}(t)}{dt} = \varepsilon \left(J - N_{res} - (N_{res} + \nu)|E_{res}|^2 \right) \quad (4)$$

with

$$\varepsilon := \frac{\tau_f}{\tau_c} \quad (5)$$

$$J := \frac{\tau_f G_N}{2} (\tau_c I + N_0) \quad (6)$$

$$\nu := \frac{\tau_f}{2\tau_p} \quad (7)$$

Note that $-\nu$ corresponds to the transparency density for the rescaled N .

In the sequel we will use only the rescaled equations (3), (4), omitting for simplicity the subscripts for the rescaled variables N and E . The feedback parameters η and ϕ will be our primary bifurcation parameters. In addition we will make use of the fact that ε is small with respect to the other coefficients. This is still true for a length of the compound cavity of some millimeters.

2 The optical equation

2.1 Rotating waves and saddle-nodes

We start with collecting some basic facts about stationary lasing states for the Lang-Kobayashi system, which can be found similarly in earlier works such as e.g. [13], [12], [11]. Looking for rotating wave solutions of the form

$$E(t) = E_s e^{i\omega_s t}, \quad N(t) = N_s \quad (8)$$

in (3), one obtains the equation

$$i\omega_s = (1 + i\alpha)N_s + \eta e^{-i(\phi + \omega_s)}. \quad (9)$$

Splitting this into real and imaginary part gives the conditions

$$N_s = -\eta \cos(\phi + \omega_s) \quad (10)$$

$$\omega_s - \alpha N_s = -\eta \sin(\phi + \omega_s), \quad (11)$$

or, plugging (10) into (11),

$$\omega_s = -\eta(\alpha \cos(\phi + \omega_s) + \sin(\phi + \omega_s)) \quad (12)$$

The carrier equation (4) may be used to determine the intensity

$$|E_s|^2 = \frac{J - N_s}{N_s + \nu},$$

but the carrier equation does not affect the conditions (10), (11) for N_s and ω_s . These rotating wave solutions are called in the literature *external cavity modes* (ECMs), and can be represented as points in the (ω, N) -plane. In our coordinates the origin in this plane corresponds to the stationary state of the laser without feedback. Then, for small feedback η , there is only one stable solution close to the origin, which under different phase conditions changes slightly its threshold density and optical

frequency. For larger feedback, the number of solutions increases and some of them may be unstable.

Indeed, from (10), (11) it is clear that in the (ω, N) -plane all ECM solutions for fixed η are located on an ellipse around zero. This ellipse grows for increasing values of η . Changing only ϕ , all the solutions move along the ellipse (see [13]). These solutions are determined only by the optical equation (3), and we can use this equation also to some extent for a study of the stability and bifurcations of the stationary points.

If ω_s is a double root of (12), then we have a saddle-node bifurcation of rotating waves. To this end we differentiate (12) with respect to ω_s and obtain

$$1 = \eta(\alpha \sin(\phi + \omega_s) - \cos(\phi + \omega_s)) \quad (13)$$

Together with the conditions (10) and (11) this gives in the (ω, N) -plane the straight line (compare [13])

$$\omega_s = \alpha N_s - \frac{1 - N_s}{\alpha} \quad (14)$$

Solutions above this line are always unstable, the solutions below may be stable or unstable. We want now to represent the condition for this bifurcation, as usually done in bifurcation theory, in the space of the main parameters η and ϕ . To this end, we first solve the transcendental equations (10), (11) for η and ϕ , obtaining

$$\eta = \sqrt{N^2 + (\omega - \alpha N)^2} \quad (15)$$

$$\phi = \begin{cases} 0 & \\ \arccos(-\frac{N}{\eta}) - \omega & \text{for } \omega - \alpha N \geq 0 \\ -\arccos(-\frac{N}{\eta}) - \omega & \text{for } \omega - \alpha N < 0 \end{cases} \quad (16)$$

and then plug in the saddle-node condition (14). In Figure 1, we have plotted the saddle-node condition (14) for fixed $\alpha = 2$, and the resulting curve in the parameter plane (compare [12]). Note that this curve has a singular point (called *cusp point*) which corresponds to a triple root of (12). Its location in the (ω, N) -plane can be computed as

$$\omega_s = 0, \quad N_s = \frac{1}{1 + \alpha^2}, \quad (17)$$

and in parameter space

$$\eta = \frac{1}{\sqrt{1 + \alpha^2}}, \quad \phi = (2k + 1)\pi - \arctan(\alpha). \quad (18)$$

This value of η is the minimal feedback which is necessary to have under an appropriate phase condition more than one ECM on the ellipse .

Of course, the phase ϕ is only determined up to addition of multiples of 2π ; looking at the interval $\phi \in [0, 2\pi]$, any bifurcation curve which leaves this interval at one side enters at the same time at the other side. At each branch of the saddle-node curve the number of solutions changes by two, leading to more and more ECMs for increasing η (see Figure 1). The situation with five ECMs on the ellipse, given in the left part of the figure corresponds to the parameter values, indicated by the cross in the right hand side of the figure.

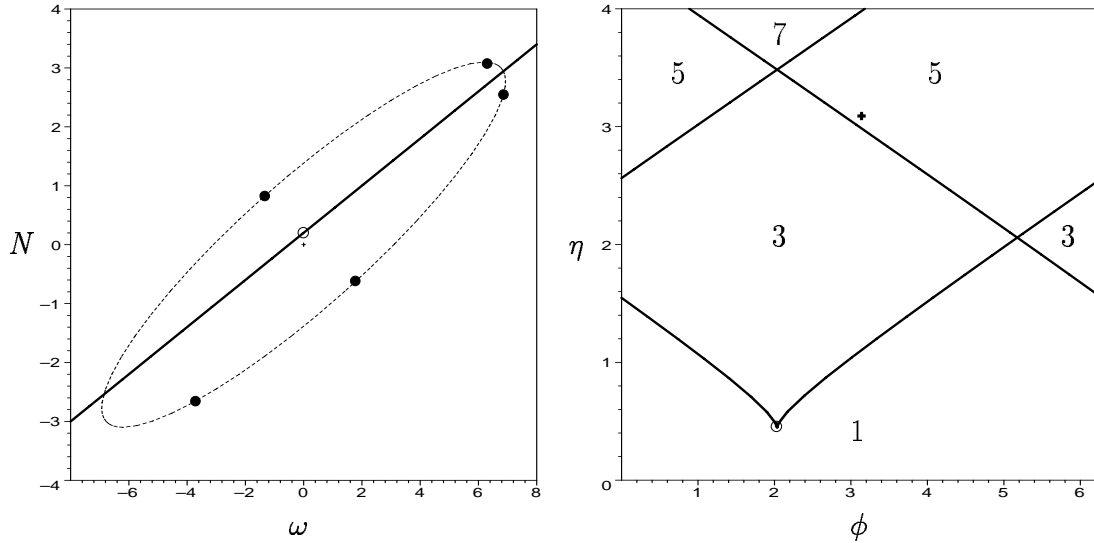


Figure 1: saddle-node curve with cusp-point (circle) for $\alpha = 2$. Left: (ω, N) -plane, ellipse for $\eta = 3.1$ with 5 ECMs for $\phi = \pi$. Right: (ϕ, η) -plane, number of ECMs

2.2 The Petermann-Tager condition

It was first observed by Petermann and Tager in [11] that the existence of two ECM with the same carrier density may lead to stable pulsations of the laser with a frequency, given by the difference of the two ECM frequencies. These numerical observations were confirmed by results of Erneux e.a., showing by asymptotic expansion techniques [3] and later also with numerical path-following techniques [8, 9] the existence of such pulsating solutions.

Here, we first want to derive an explicit condition for the existence of two ECMs with equal N . This can be done again using only the optical equation (3). We start with two copies of the equations (10) and (11)

$$N_{1,2} = -\eta \cos(\phi + \omega_{1,2}) \quad (19)$$

$$\omega_{1,2} - \alpha N_{1,2} = -\eta \sin(\phi + \omega_{1,2}), \quad (20)$$

Assuming $N := N_1 = N_2$ and $\omega_1 \neq \omega_2$, the equations (19) give

$$\omega_1 + \phi = 2k\pi - (\omega_2 + \phi). \quad (21)$$

Adding now the two equations (20) yields

$$\frac{\omega_1 + \omega_2}{2} = \alpha N, \quad \text{or} \quad \frac{\omega_1 - \omega_2}{2} = \omega_1 - \alpha N \quad (22)$$

Inserting the relation (21) gives

$$\phi = k\pi - \alpha N. \quad (23)$$

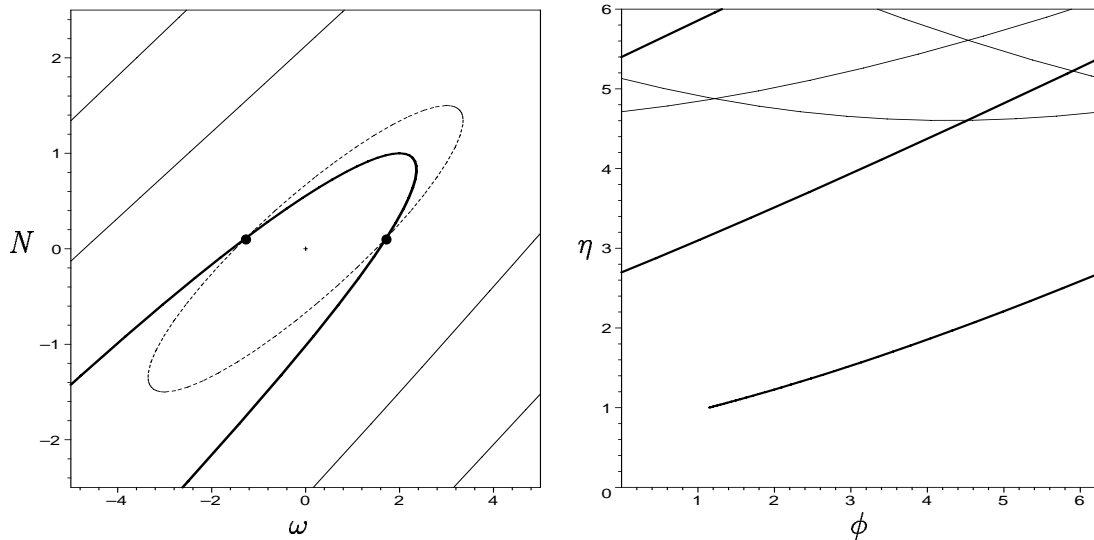


Figure 2: Petermann-Tager condition (24) for $\alpha = 2$. Left: (ω, N) -plane; an arbitrary ECM ellipse for $\eta > 1$ intersects the curve at two ECM solutions with equal N . Right: (ϕ, η) -plane; due to the periodicity of ϕ the first (thick line) and second branch (thin line) appear repeatedly in the interval $\phi \in [0, 2\pi]$

Since we excluded the case $\omega_1 = \omega_2$, corresponding to $\omega_1 - \alpha N = 0$ (see (22)), we may divide (19) by (20) to eliminate η , giving finally

$$N = (\omega_1 - \alpha N) \cot(\omega_1 - \alpha N). \quad (24)$$

In Figure 2, we have plotted the resulting curve for $\alpha = 2$ in the (ω, N) -plane and, using again (15), (16), also in the (ϕ, η) -plane of our primary bifurcation parameters. According to (24), a variation of the parameter α does not change the picture qualitatively. At the intersection points of the different solution branches in the parameter plane, we have two coexisting pairs of PT modes. However, the picture in the (ω, N) -plane indicates that the pair from the first branch should have the lowest threshold density. At the other hand, the existence of a stable pulsating solution can be expected only, if one mode of the PT pair is stable.

2.3 Mode degeneracy

Writing the condition (9) for rotating wave solutions as

$$\lambda = (1 + i\alpha)N_s + \eta e^{-i\phi} e^{-\lambda} \quad (25)$$

with a complex spectral parameter λ instead of ω_s , it turns out to be the characteristic equation for the linear delay differential equation (3), depending parametrically on N . Hence, the ECM frequencies ω_s are eigenvalues λ which are in addition pure imaginary. An optical mode degeneracy occurs, if there is a double eigenvalue, i.e.

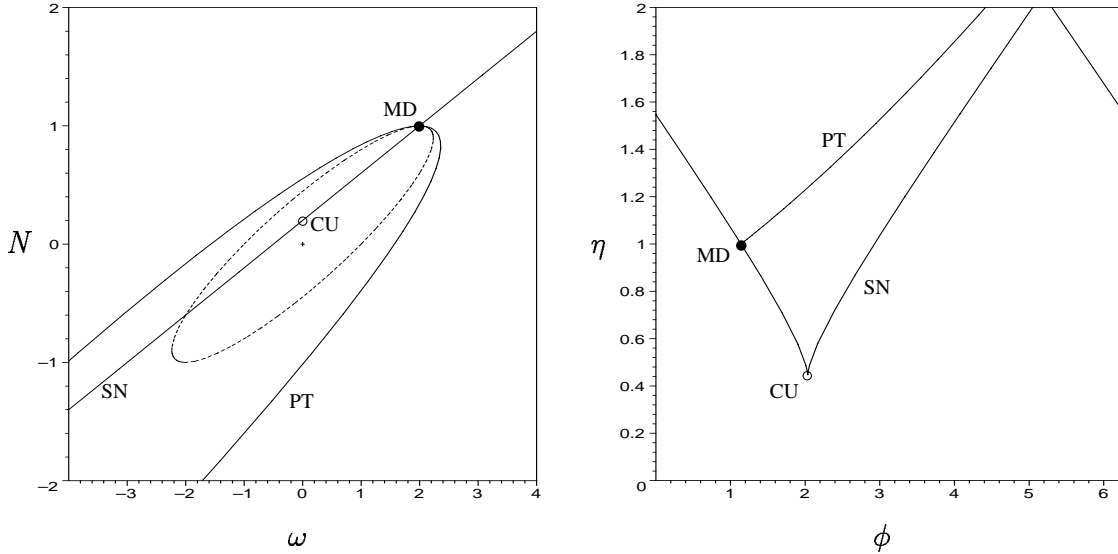


Figure 3: Petermann-Tager (PT) and saddle-node bifurcation (SN) curves, mode-degeneracy (MD) and cusp-point (CU) in the (ω, N) -plane (left) and in the (ϕ, η) -plane (right)

a double root of (25). Differentiating (25) by λ , we obtain

$$1 = -\eta e^{-i\phi} e^{-\lambda}.$$

Together with (25) this has the unique solution $\lambda = (1 + i\alpha)N - 1$, which is pure imaginary exactly for $N = 1$, giving $\lambda = i\omega_s = i\alpha$. This point with a degenerate ECM solution plays an important role for the dynamics of the system. Note that the saddle-node condition (14) is satisfied there. Also the first branch of the PT curve limits to this point, indicating that two ECM with equal N_s merge in the degeneracy point with the frequency difference going to zero. Correspondingly, there is a point of tangency of the ECM ellipse for $\eta = 1$ and the PT curve (see left part of Figure 3).

There are also further intersections between the PT curve and the saddle-node curve, however, without a mode degeneracy. They also lead to interesting bifurcations, but shall not be studied here, since they occur at much higher feedback levels.

3 Linearized dynamics at external cavity modes

After having obtained so far a lot of information from the optical equation (3) alone, we proceed in our stability and bifurcation analysis of the external cavity modes by considering now the full system, including also the carrier equation (4). For the theoretical background of our treatment of nonlinear differential delay systems we refer to [4], [15].

First, we introduce for a particular ECM solution

$$E(t) = E_s e^{i\omega_s t}, \quad N(t) = N_s, \quad (26)$$

where ω_s, N_s, E_s satisfy the ECM conditions (9), the corotating coordinates

$$E_{new}(t) = e^{-i\omega_s t} E(t).$$

Then the rotating wave solution (26) becomes a stationary state of the transformed system

$$\dot{E}_{new}(t) = ((1 + i\alpha)N - i\omega_s) \cdot E_{new}(t) + \eta e^{-i(\phi + \omega_s)} \cdot E_{new}(t - 1) \quad (27)$$

$$\dot{N}(t) = \varepsilon(J - N - (N + \nu)|E_{new}(t)|^2). \quad (28)$$

Splitting the equation for the optical field amplitude into real and imaginary part as $E_{new}(t) = x(t) + iy(t)$, we obtain

$$\dot{x}(t) = (x(t) - \alpha y(t))N + \omega_s y(t) + \eta[x(t - 1) \cos(\phi + \omega_s) + y(t - 1) \sin(\phi + \omega_s)]$$

$$\dot{y}(t) = (\alpha x(t) + y(t))N - \omega_s x(t) + \eta[y(t - 1) \cos(\phi + \omega_s) - x(t - 1) \sin(\phi + \omega_s)]$$

$$\dot{N}(t) = \varepsilon(J - N - (N + \nu)(x(t)^2 + y(t)^2).$$

This system can now be easily linearized in the form

$$\frac{d}{dt} \vec{v}(t) = A \vec{v}(t) + B \vec{v}(t - 1)$$

with $\vec{v} = (v_1, v_2, v_3)$ corresponding to variation of x, y, N , respectively. The matrices A and B can be computed as

$$A = \begin{pmatrix} N & \omega_s - \alpha N & x - \alpha y \\ -(\omega_s - \alpha N) & N & \alpha x + y \\ -2\varepsilon x(N + \nu) & -2\varepsilon y(N + \nu) & -\varepsilon(1 + x^2 + y^2) \end{pmatrix} \quad (29)$$

$$B = \begin{pmatrix} \eta \cos(\phi + \omega_s) & \eta \sin(\phi + \omega_s) & 0 \\ -\eta \sin(\phi + \omega_s) & \eta \cos(\phi + \omega_s) & 0 \\ 0 & 0 & 0 \end{pmatrix} \quad (30)$$

The characteristic equation for the eigenvalues of this linear system is now given by the transcendental equation

$$\begin{aligned} \chi(\Lambda) &= \det(\Lambda \text{Id} - A - e^{-\Lambda} B) = \\ &= \left[(\Lambda - N - e^{-\Lambda} \eta \cos(\phi + \omega_s))^2 + (\omega_s - \alpha N + e^{-\Lambda} \eta \sin(\phi + \omega_s))^2 \right] (\Lambda + \varepsilon(1 + x^2 + y^2)) \\ &+ 2\varepsilon(x^2 + y^2)(N + \nu) \left[\Lambda - (1 + \alpha^2)N + \alpha\omega_s + e^{-\Lambda} \eta (\alpha \sin(\phi + \omega_s) - \cos(\phi + \omega_s)) \right] \end{aligned}$$

with the complex spectral parameter Λ . Using the ECM conditions

$$|E_s|^2 = x^2 + y^2, \quad N = N_s = -\eta \cos(\phi + \omega_s), \quad \omega_s - \alpha N_s = -\eta \sin(\phi + \omega_s)$$

we obtain the characteristic equation for the linearization at the ECM solution as

$$\begin{aligned} \chi(\Lambda) &= \left[(\Lambda + N_s(e^{-\Lambda} - 1))^2 + (\omega_s - \alpha N_s)^2 (e^{-\Lambda} - 1)^2 \right] (\Lambda + \varepsilon(1 + |E_s|^2)) \\ &+ \left[\Lambda + ((1 + \alpha^2)N_s - \alpha\omega_s)(e^{-\Lambda} - 1) \right] 2\varepsilon |E_s|^2 (N_s + \nu) \end{aligned} \quad (31)$$

3.1 The Hopf condition

For a Hopf bifurcation it is necessary to have pair of pure imaginary solutions to (31), i.e.

$$\chi(\Lambda) = 0, \quad \Lambda = i\Omega, \quad \Omega \in \mathbf{R}$$

The resulting equation can again be split into real part

$$\begin{aligned} 0 = & 2\Omega(\cos \Omega - 1) \left[\sin \Omega (N_s^2 + (\omega_s - \alpha N_s)^2) - \Omega N_s \right] \\ & + \varepsilon(1 + |E_s|^2) \left[-\Omega^2 + 2 \cos \Omega (\cos \Omega - 1) (N_s^2 + (\omega_s - \alpha N_s)^2) + 2 N_s \Omega \sin \Omega \right] \\ & + 2\varepsilon |E_s|^2 (N_s + \nu) ((1 + \alpha^2) N_s - \alpha \omega_s) (\cos \Omega - 1) \end{aligned} \quad (32)$$

and imaginary part

$$\begin{aligned} 0 = & \Omega \left[-\Omega^2 + 2 \cos \Omega (\cos \Omega - 1) (N_s^2 + (\omega_s - \alpha N_s)^2) + 2 N_s \Omega \sin \Omega \right] \\ & - 2\varepsilon(1 + |E_s|^2) (\cos \Omega - 1) \left[\sin \Omega (N_s^2 + (\omega_s - \alpha N_s)^2) - \Omega N_s \right] \\ & + 2\varepsilon |E_s|^2 (N_s + \nu) (\Omega - ((1 + \alpha^2) N_s - \alpha \omega_s) \sin \Omega). \end{aligned} \quad (33)$$

Note that, due to the phase shift invariance of the rotating waves, zero always solves the eigenvalue equation (31). Moreover, zero is a double solution to (31) exactly at the saddle node curve (14). Correspondingly, $\Omega = 0$ is exactly there also a solution to the equations (32), (33).

3.2 Approximate solutions by scaling methods

In order to find analytically further solutions to (32), (33), we use the smallness of ε . Assuming that there are solutions where Ω stays away from zero also for ε tending to zero, we can put $\varepsilon = 0$. From the remaining terms

$$\begin{aligned} 0 &= \sin \Omega (N_s^2 + (\omega_s - \alpha N_s)^2) - \Omega N_s \\ 0 &= -\Omega^2 + 2 \cos \Omega (\cos \Omega - 1) (N_s^2 + (\omega_s - \alpha N_s)^2) + 2 N_s \Omega \sin \Omega, \end{aligned} \quad (34)$$

we obtain immediately that

$$N_s = -\frac{\Omega \sin \Omega}{2(\cos \Omega - 1)} \quad (35)$$

$$\omega_s - \alpha N_s = \frac{\Omega}{2} \quad (36)$$

$$N_s = (\omega_s - \alpha N_s) \cot(\omega_s - \alpha N_s) \quad (37)$$

This result is the same which we get from the Petermann-Tager condition (24) for the existence of two ECM solutions with the same threshold value. Moreover, the Hopf-frequency Ω coincides with the difference of the two ECM frequencies (compare (36) and (22)). It was already noticed in [3] that the Petermann-Tager condition

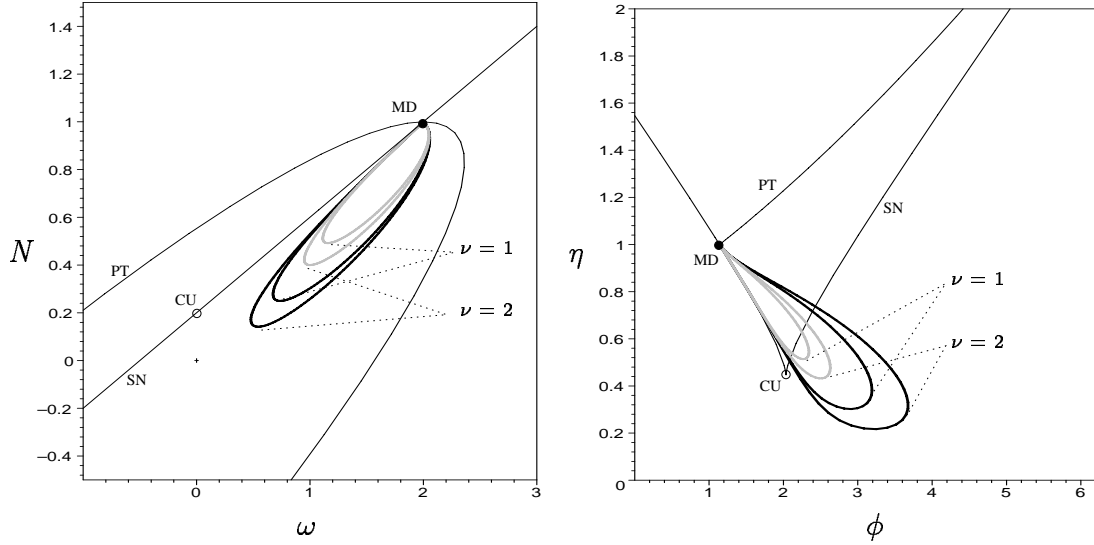


Figure 4: Thick lines: Bifurcation curves for the DQS-Hopf ($\alpha = 2$). Grey: low intensity ($|E|^2 = 0.2$), black: high intensity ($|E|^2 = 2$)

coincides with the zero order approximation of the Hopf-condition. With Figure 2, we give here the bifurcation curves both in the (ω, N) - and (ϕ, η) -plane. Note that the two branches of solutions to (37) which emanate from the point of mode degeneracy in the (ω, N) -plane, are mapped to the same branch in the (ϕ, η) -plane. If first order corrections in ε are taken into account, this coincidence will disappear, and two Hopf-branches, both close to the approximate curve will appear. This coincides also with the results in [8], where for changing η corresponding pairs of Hopf points have been found near the PT condition.

But in addition to these solutions, we get another type of solutions to (32) and (33), if we assume that Ω^2/ε remains finite for ε tending to zero (compare [14]). Here we may replace trigonometric functions by Taylor expansions and obtain for the rescaled variable

$$\Omega_r = \frac{\Omega}{\sqrt{\varepsilon}}$$

in leading order of ε the equations

$$\begin{aligned} 0 &= \Omega_r^2(N_s - N_s^2 - (\omega_s - \alpha N_s)^2) - (1 + |E_s|^2)((N_s - 1)^2 + (\omega_s - \alpha N_s)^2) - \\ &\quad |E_s|^2(N_s + \nu)((1 + \alpha^2)N_s - \alpha\omega_s) \\ 0 &= -\Omega_r^2((N_s - 1)^2 + (\omega_s - \alpha N_s)^2) + 2|E_s|^2(N_s + \nu)(1 - N_s + \alpha(\omega_s - \alpha N_s)). \end{aligned}$$

Eliminating Ω_r^2 , and using the new coordinates

$$\bar{n} = 1 - N_s, \quad \bar{\omega} = \omega_s - \alpha N_s, \quad (38)$$

we get the Hopf condition

$$-\frac{1}{|E_s|^2} = 1 + (1 - \bar{n} + \nu) \left(\frac{\bar{n} + \alpha\bar{\omega}}{\bar{n}^2 + \bar{\omega}^2} - \frac{(\bar{n} + \alpha\bar{\omega})^2 - (1 + \alpha^2)\bar{\omega}^2}{(\bar{n}^2 + \bar{\omega}^2)^2} \right). \quad (39)$$

The corresponding Hopf-frequency is given by

$$\Omega^2 = \varepsilon \frac{2|E_s|^2(N_s + \nu)(\bar{n} + \alpha\bar{\omega})}{\bar{n}^2 + \bar{\omega}^2}. \quad (40)$$

From this, we get the constraint $\bar{n} + \alpha\bar{\omega} > 0$ in addition to the condition (39). Note that according to (40) the Hopf frequency along this branch of solutions is comparable to the relaxation frequency

$$\Omega^2 \approx \Omega_{rel}^2 = \varepsilon|E_s|^2\nu$$

of the solitary laser. Hence we can interpret this branch of Hopf-bifurcations as an undamping of the relaxation oscillation. Similar phenomena in two-section DFB lasers were called in [1] DQS-pulsations (dispersive self Q-switching). Here, obviously the Fabry-Perot dispersion of the external cavity leads to this type of instability.

We have plotted in Figure (4) this DQS-Hopf curve, together with the bifurcation curves, calculated before. The figure shows also the dependence of the DQS-Hopf curve on the intensity $|E_s|^2$, which is of course related with the pumping J , and the parameter ν (transparency level), which originate from the carrier rate equation (4) and do not influence the bifurcation curves, computed above.

Note that this curves again start and end at the point of mode degeneracy

$$\bar{n} = \bar{\omega} = 0.$$

There, however, both the limits of finite Ω and $\Omega = O(\sqrt{\varepsilon})$ are not valid, so that both the PT and DQS curves do not give a correct approximation of solutions to the Hopf condition (32), (33). To derive an approximate formula for the Hopf bifurcation curves near the mode degeneracy point, one should notice that near this point both the quantities Ω and $\frac{\varepsilon}{\Omega^2}$ are small. Note also that the closeness to the mode degeneracy point means that the quantities \bar{n} and $\bar{\omega}$ are small as well. By expanding in powers of Ω , $\frac{\varepsilon}{\Omega^2}$, \bar{n} and $\bar{\omega}$, and omitting higher order terms, we obtain from equation (32) the approximate relation

$$\bar{n} - \bar{\omega}^2 - \frac{\varepsilon}{\Omega^2}S(1 + \nu) + \frac{\Omega^2}{6} \approx 0,$$

and from (33) the approximate relation

$$\frac{\Omega^2}{4} - \bar{n}^2 - \bar{\omega}^2 + 2\frac{\varepsilon}{\Omega^2}S(1 + \nu)(\alpha\bar{\omega} + \bar{n}) \approx 0.$$

To the leading order in Ω and $\frac{\varepsilon}{\Omega^2}$ these equations give

$$\bar{n} \approx \frac{\varepsilon}{\Omega^2}S(1 + \nu) + \frac{\Omega^2}{12},$$

$$\bar{\omega} \approx \alpha \frac{\varepsilon}{\Omega^2} S(1 + \nu) \pm \sqrt{\left(\frac{\varepsilon}{\Omega^2} S(1 + \nu)\right)^2 (1 + \alpha^2) + \frac{\Omega^2}{4}}.$$

Note that we have here two disjoint branches of the Hopf bifurcation curve. At small Ω and $\frac{\varepsilon}{\Omega^2}$ we get small \bar{n} and $\bar{\omega}$, i.e. these branches are indeed close to the mode degeneracy point ($N = 1, \omega = \alpha$). Each branch is parametrized by the value of Ω which runs monotonically from $O(\sqrt{\varepsilon})$ to small finite values, i.e. each branch connects one of the ends of the DQS-type Hopf-curve with one of the two Petermann-Tager curves.

It should also be noted that the “minus” branch intersects the saddle-node curve $\bar{\omega} = -\bar{n}/\alpha$ (cf. equation (14)). Indeed, the equation for the intersection point is

$$-\frac{\varepsilon}{\alpha\Omega^2} S(1 + \nu) - \frac{\Omega^2}{12\alpha} \approx \alpha \frac{\varepsilon}{\Omega^2} S(1 + \nu) - \sqrt{\left(\frac{\varepsilon}{\Omega^2} S(1 + \nu)\right)^2 (1 + \alpha^2) + \frac{\Omega^2}{4}},$$

which gives indeed a unique solution

$$\Omega^3 \approx 2\varepsilon \frac{S(1 + \nu)}{\alpha} \sqrt{1 + \alpha^2}.$$

This intersection point (called “fold-Hopf interaction”, or “Gavrilov-Guckenheimer point”) is remarkable because its presence implies further nontrivial dynamics, such as bifurcation of invariant tori and homoclinic phenomena (see e.g.[5]). In fact, also the curve of torus bifurcation, which has been found in [9], seems to be a consequence of this point.

3.3 Numerical solutions for the Hopf condition

After having studied analytically the two types of Hopf-bifurcations and their transition regime near the point of mode degeneracy, we present now some numerical results: Figure 5 shows our numerical solution to the system of equations (32), (33) for fixed values of the secondary parameters $\alpha, \nu, \varepsilon, |E|^2$. To make differences to the asymptotic curves (in the Figure dashed) better visible, we have chosen $\varepsilon = 0.01$ only of moderate smallness. Apart from the point of Mode-Degeneracy, the computed curve shows a good coincidence with the asymptotic PT and DQS curve.

Note that there are indeed two branches of the Hopf curve, both approaching the PT curve in the (ϕ, η) -plane). Each of them is connected with one of the two ends of the DQS curve. Moreover, one can see that in the vicinity of the mode degeneracy one branch of the Hopf curve meets the saddle-node line in a point of tangency (fold-Hopf interaction). Recall that in the (ω, N) -plane the region above the saddle-node line contains the ECM solutions of saddle type, whereas below the saddle-node line the nodes are located. This corresponds to the well known fact that at a fold-Hopf interaction point the type of the bifurcating equilibrium changes along the Hopf curve [5].

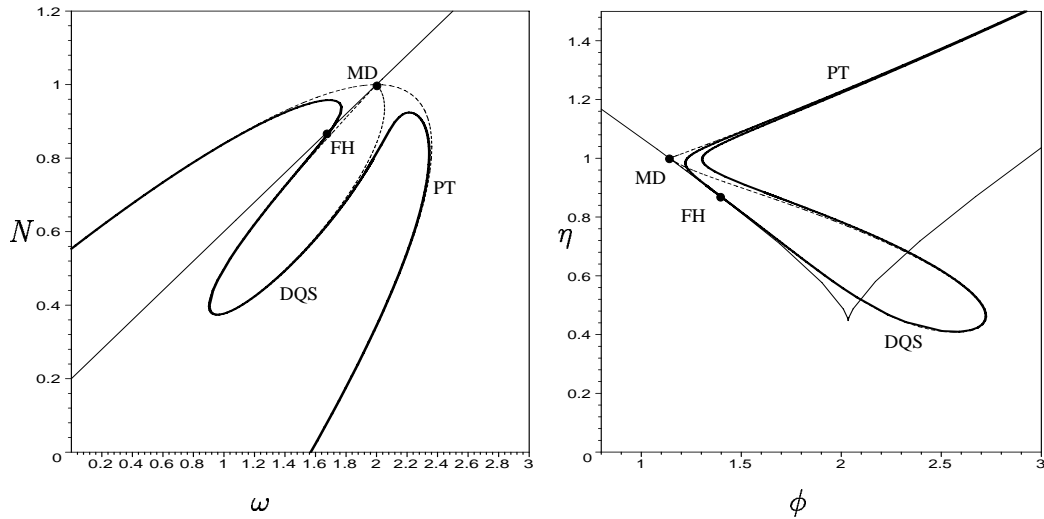


Figure 5: Numerically obtained Hopf curves for $\varepsilon = 0.01$, $\nu = 1$, $|E|^2 = 0.5$ (left: (ω, N) -plane, right: (η, ϕ) -plane); dashed: curves from the asymptotic approximations (34), and (39); thin line: saddle-node curve; FH; fold-Hopf interaction

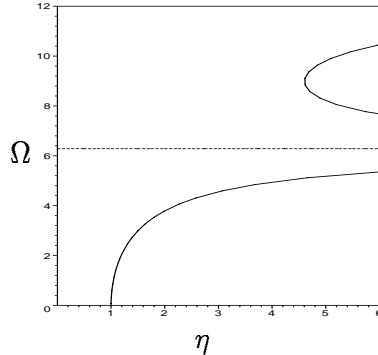


Figure 6: PT Hopf frequency Ω for changing feedback level η , according to (41).

As an organizing center of the whole scenario acts the point of optical Mode Degeneracy. It separates the two different regimes of DQS and PT pulsations, and leads to the nearby fold-Hopf interaction as well as to a second appearance of the Hopf curve in the vicinity of this point, exactly where the frequency on this branch changes from order $\sqrt{\varepsilon}$ to order 1. Since for the PT pulsation, the Hopf frequency is given by the beating frequency of the two modes, we can calculate explicitly the relation of this frequency Ω and the feedback level η : Inserting (36) and (23) into (11), we obtain

$$\eta = \left| \frac{\Omega}{2 \sin(\frac{\Omega}{2})} \right| \quad (41)$$

Note that apart from the specific scaling of η and the time unit, there enters no specific parameter into this formula. Figure 6 shows that the PT frequency on the first branch is tunable between zero and the value 2π in our rescaled time. However,

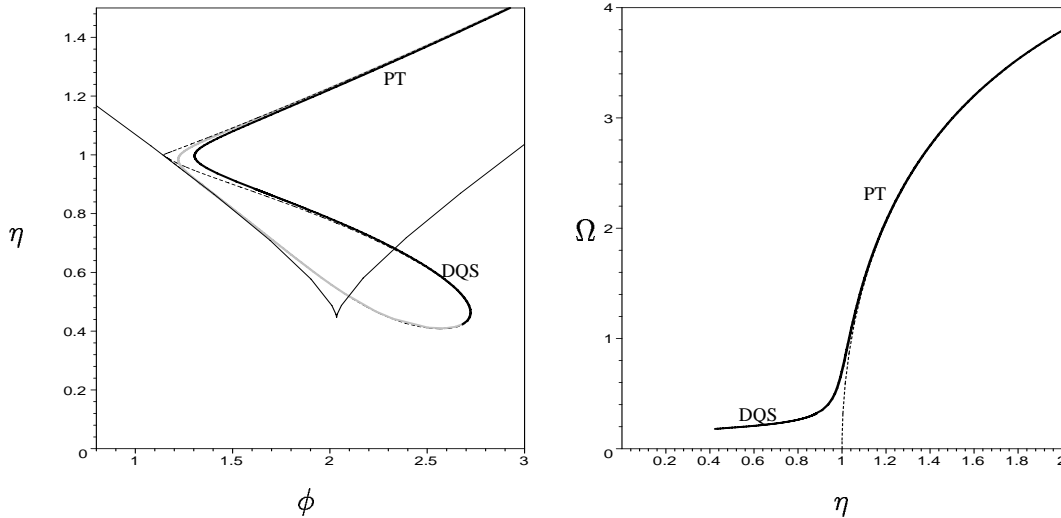


Figure 7: Right: Hopf frequency Ω for changing feedback level η along the part of the Hopf curve indicated in black at the right (dashed: asymptotic approximation for PT frequency, cf. Figure 6)

it is necessary to meet the appropriate phase condition. For larger η there appear also more and more pairs of PT modes with larger frequency difference, the first of which leads to the second branch in Figure 6.

In Figure 7 we show also the numerically obtained Hopf frequency along the part of the Hopf curve, connecting with increasing η the DQS and the PT regime. One can observe, that for $\eta < 1$ (i.e. the DQS case) the frequency is indeed of order $\sqrt{\varepsilon}$. Then, after an intermediate regime around $\eta = 1$, the curve follows the curve given by (41).

4 Conclusions

We have studied Hopf bifurcations, leading to pulsation instability of lasers with optical feedback. Restricting to a moderate feedback time, one can distinguish two different types of pulsations, the DQS- and Petermann-Tager (PT) pulsations. The frequency of the first type is related to the relaxation frequency of the solitary laser, whereas for the second type it is determined by the frequency difference of two external cavity modes with the same threshold density. The occurrence of these two types of pulsations is separated by a distinguished feedback level (in our rescaled variables $\eta = 1$). Using the ratio of feedback time and carrier lifetime as a small parameter, we were able to compute explicit expressions for the bifurcation curves, showing also the influence of secondary parameters. Moreover, we studied the transition from one type to the other, which is organised by the point of mode degeneracy and comes along with a codimension-two bifurcation of Guckenheimer-Gavrillov type (fold-Hopf interaction). This codimension two bifurcation is known

to give rise to a lot of complicated dynamics and nonlocal bifurcations.

The two presented mechanisms for pulsations seem to be fundamental for laser devices where a moderately delayed feedback is present. Especially the role of the point of mode degeneracy as an organizing center for the different types of pulsations seems to be a more general feature [14]. Indeed, similar bifurcation scenarios have been obtained in [10] for three-section lasers with one active section. These results, however, are based on a time domain model, and have been obtained by center manifold techniques and numerical path-following of bifurcation curves.

The high frequency pulsations of the PT type (for appropriate device parameters more than 40 GHz should be possible), together with the shown tunability of their frequency seem to be a promising feature for applications in optical communication technique.

References

- [1] U. Bandelow, H.-J. Wünsche, B. Sartorius, M. Möhrle, *Dispersive Self Q-Switching in DFB Lasers, Theory versus Experiment*, IEEE J. Selected Topics in Quantum El. Vol. 3, (1997), 270-278.
- [2] R.L. Davidchack, Y.-C. Lai, A. Gavrielides, V. Kovanis, *Chaotic transitions and low-frequency fluctuations in semiconductor lasers with optical feedback*, Pys. D 145, (2000), 130-143.
- [3] T. Erneux, F. Rogister, A. Gavrielides, V. Kovanis, *Bifurcation to mixed external cavity mode solutions for semiconductor lasers subject to optical feedback* Opt. Comm. 183 (2000), 476-477.
- [4] J. K. Hale, S. M. Verduyn Lunel, *Introduction to Functional Differential Equations*, Appl. Math. Sci. 99, Springer, New York (1993).
- [5] Y.A. Kusnetsov, *Elements of Applied Bifurcation Theory*, Appl. Math. Sci. 112, New York, (1995).
- [6] R. Lang, K. Kobayashi, *External optical feedback effects on semiconductor injection laser properties*, IEEE J. Quant. El. 16, (1980), 347-355.
- [7] J. Mørk, B. Tromborg, J. Mark, *Chaos in Semiconductor Lasers with Optical Feedback: Theory and Experiment*, IEEE J. Quantum Elect. Vol. 28, No. 1, (1992) 93-108.
- [8] D. Pieroux, T. Erneux, B. Haegeman, K. Engelborghs, D. Roose, *Bridges of Periodic Solutions and Tori in Semiconductor Lasers Subject to Delay*, Phys. Rev. Let. Vol. 87, No. 19, (2001).

- [9] D. Pieroux, T. Erneux, T. Luzyanina, K. Engelborghs, D. Roose, *Interacting pairs of periodic solutions lead to tori in lasers subject to delayed feedback*, Phys. Rev. E, Vol. 63, No.3, (2001).
- [10] J. Sieber, *Numerical bifurcation analysis for multi-section semiconductor lasers*, WIAS-Preprint No. 683, Berlin, (2001).
- [11] A. A. Tager, K. Petermann, *High-Frequency Oscillations and Self-Mode Locking in Short External-Cavity Laser Diodes*, IEEE J. Quantum Elect. Vol. 30, No. 7, (1994) 1553-1561.
- [12] G.H.M. van Tartwijk, G.P. Agrawal, *Laser instabilities: a modern perspective*, Prog. in Quant. El. 22, (1998), 43-122.
- [13] B. Tromborg, J. H. Osmundsen, H. Olesen, *Stability Analysis for a Semiconductor Laser in an External Cavity*, IEEE J. Quantum Elect. Vol. 20, No. 9, (1984) 1023-1032.
- [14] D. Turaev *Fundamental obstacles to self-pulsations in low-intensity lasers*, WIAS-Preprint N0. 629, (2001).
- [15] S.M. Verduyn Lunel, B. Krauskopf, *The Mathematics of Delay equations with an Application to the Lang-Kobayashi Equations*, in AIP Conf. Proc. 548, (2000).